



# XI Congreso Ibérico de Agroingeniería XI Congresso Ibérico de Agroengenharia 2021



Type of the Paper (Paper)

## Forest Species Mapping using Sentinel 2A images for the Central Alentejo Region (Portugal)

Crismeire Isbaex <sup>1</sup>, Adélia M. O. Sousa <sup>2</sup>, Ana Cristina Gonçalves <sup>2</sup>

<sup>1</sup> Departamento de Engenharia Rural, Escola de Ciências e Tecnologia, Instituto de Investigação e Formação Avançada, Universidade de Évora, Apartado 94, 7002-544 Évora, Portugal. E-mail: cisbaex@uevora.pt.

<sup>2</sup> Departamento de Engenharia Rural, Escola de Ciências e Tecnologia, Instituto Mediterrânico de Agricultura, Ambiente e Desenvolvimento (MED), Instituto de Investigação e Formação Avançada, Universidade de Évora, Apartado 94, 7002-544 Évora, Portugal. E-mail: asousa@uevora.pt, acag@uevora.pt

**Abstract:** In past years, studies about Land Use and Land Cover (LULC) have been approached extensively in remote sensing for providing information on the environmental and global changes in the landscape. In the forest species mapping, one of the major challenges when using Sentinel-2 (S2A) multispectral data is to delineate and discriminate areas of heterogeneous forest components with spectral similarity at the canopy level. In this context, the main objective of this study was to evaluate the S2A data performance for LULC mapping, using a Random Forest classifier (RF). A set of 26 independent variables derived from the 2019 summer period S2A data, with a spatial resolution of 10 m, was used. A total of eight object-based LULC classes were created, four forest classes (*Quercus suber*, *Quercus rotundifolia*, *Eucalyptus sp*, and *Pinus pinea*) and four other uses. For this propose supervised classification method was applied using the RF classifier. The cartography accuracy assessment was performed using the statistics confusion matrix and Kappa coefficient (k). This study showed that the RF classifier achieved high overall accuracy (92%) and Kappa (91%) for the four forest classes defined using S2A data.

**Keywords:** cartography; forest occupation; supervised classification.

### 1. Introduction

The LULC mapping using remote sensing techniques has been widely used to describe the composition and distribution of natural elements on the Earth's surface. In addition, the thematic maps reflect political decision-making on land use planning and, above all, the human activities' effects on the forest resources. In Mediterranean ecosystems, one of the great challenges is to produce accurate LULC maps from complex data collected in areas with high landscape fragmentation [1]. The identification and spatial distribution of forest species are essential to prevent and control large-scale forest fires. In mainland Portugal, the forest occupation is the main land use, which corresponds to 36% of the territory, followed by areas of woods and pastures (31%), agricultural area (24%), urban use (5%), unproductive and inland waters (2% each) [2]. In this context, it is important to investigate the potential of remote sensing data for the mapping of Mediterranean ecosystems, for the possibility of providing valuable information on the forest species distribution that predominate in the landscape. For these reasons, maps contribute as an intermediate step in more complex analyses, such as landscape modeling, forest biomass estimation, and environmental monitoring [3,4].

In recent decades, significant changes in remote sensing have increased the satellite images available that facilitates the Earth's surface monitoring in a more economical and technically feasible way at regular time intervals [5]. Several satellite types are available on open access platforms, as well as several non-commercial software packages have image analysis tools [6–8]. In June 2015, the Sentinel-2A (S2A) multispectral sensor (MSI) began its mission to monitor vegetation, with a five-day revisit time, open database resources, and high spatial resolution [9]. The MSI has 13 spectral bands, with a range wavelength from 443 to 2190 nm, covering areas of the visible spectrum (V), vegetation red edge bands (Red-edges), near-infrared (NIR), narrow infrared (Narrow NIR) and short wave infrared (SWIR) [9]. The spatial resolution of the data varies according to the band: B2, B3, B4 (V), and B8 (NIR) are provided at 10 m; B5, B6, B7, (Red-edges), B8a (Narrow NIR) B11, and B12 (SWIR) are provided at 20m and B1, B9 and B10 are 60m of spatial resolution. In addition, the S2A product offers corrected reflectance images at the base of the atmosphere (Bottom Of Atmosphere-BOA) [9]. Compared to the Landsat mission, Sentinel 2 advantages are presenting a larger spectral bands volume and surpassing the MODIS data in terms of spatial resolution (10–20 m vs. 250 m) [10].

In addition to spectral information, vegetation and texture indices have improved LULC classes discrimination and classifier accuracy statistics [11,12]. Briefly, vegetation indices such as Green Normalized Difference Vegetation Index (GNDVI), Soil adjusted Vegetation Index (SAVI), Enhanced Vegetation Index (EVI), Normalized Difference Infrared Index (NDII), Normalized Difference Vegetation Index red-edge 1 narrow (NDRE 1) Normalized Difference Vegetation Index red-edge 2 narrow (NDRE 2) and Red-edge Chlorophyll Index (CI), can be used in images captured during the summer period. These indices gather combinations of pattern-sensitive bands diverging from the spectral response in semiarid environments [13]. GNDVI has the ability to be five times more sensitive to variation in chlorophyll content by using a green band rather than a red band [14]; EVI is sensitive in regions with high biomass concentration [15]; NDII determines the water content of vegetation and plant water stress using the SWIR band [16]; SAVI reduces the effects of ground pixels[17]; NDRE 1 and 2 are sensitive to small changes in the canopy, gap fraction, and senescence relative to red and green reflectance [18] and CI estimates the chlorophyll content of leaves based on the reflectance in narrow red-edged spectral bands [19].

Texture measurements describe heterogeneity in the tonal values of pixels within a defined area of an image and can be used to identify objects or regions of interest [20]. For LULC classification purposes, the texture measurements of a Gray Level Co-occurrence Matrix (GLCM), proposed by [21], has been the most adopted method for providing additional information when the spectral information is not sufficient for heterogeneous landscape classification [20]. Second-order statistics, such as the GLCM method, consists on a co-occurrence matrix that uses the relationship between neighboring pixels to characterize the texture [22]. The GLCM method analyzes the existing co-occurrences between each pair of pixels in an image, that is, it analyzes the spatial relationship between a set of pixels (given a distance and different angles) [21,23]. As an independent source of information from spectral value data, the inclusion of GLCM measurements generally improves the accuracy of classification images [1,24,25]. Among the approaches in the literature, GLCM textures can be calculated from the principal components (Principal Component Analysis - PCAs) of the spectral bands set or vegetation indices [13,23]. This strategy has as main objective to simplify and reduce the number of independent variables and correlated information [26].

Additionally the characteristics of the image, another important point must be considered, is the selection of training samples and classification methods in order to obtain an accurate classification. In Mediterranean ecosystems, where there is great structural and botanical diversity with high spectral variability [27], supervised classification methods based on machine learning methods/techniques have attracted the attention for being able to deal with large volumes of complex and non-parametric data [28,29]. In supervised mode, classification algorithms determine a LULC class based on training the spectral signatures of user-selected LULC classes, where object-based discrimination includes different land cover labels [6,12,30]. More information on supervised classification methods can be found in [31]. In LULC classification studies with Sentinel 2A images, Random Forest (RF) has been more used algorithm for attaining better performances are achieved when compared to other classifiers [3,29,32–34]. When generating a thematic map, statistical analyzes to assess accuracy can be obtained through the confusion matrix. The confusion matrix is a square matrix that, through the correlation of information from the reference data (understood as soil truth) with the classified data, assigns statistical values of the quality of the digital image classification [35]. In this way, accuracy values such as overall, user, and producer accuracy and Kappa statistic can be derived from this matrix, being useful in the interpretation of the degree of precision and coherence of a resulted thematic map [36–38].

In this context, the main objective of this study was to evaluate the performance of S2A data for LULC mapping, using the RF classifier, for mapping the forest occupation in Central Alentejo region, Portugal.

## 2. Materials and Methods

### 2.1. Description of the study area

This study was conducted in Central Alentejo (NUT-Nomenclature of Territorial Units for Statistical Purposes III region)[39], located in the south of mainland Portugal, with a territorial extension of 7 393 Km<sup>2</sup> (Figure 1). This region characterized by Mediterranean climate, with hot, dry summers (June to September) and cold, rainy winters (October to January). The forest occupation has around 338.53 thousand ha, the predominant species are *Quercus suber* (53%), *Quercus rotundifolia* (35%), *Eucalyptus sp.* e *Pinus pinea* in low percentage [2].

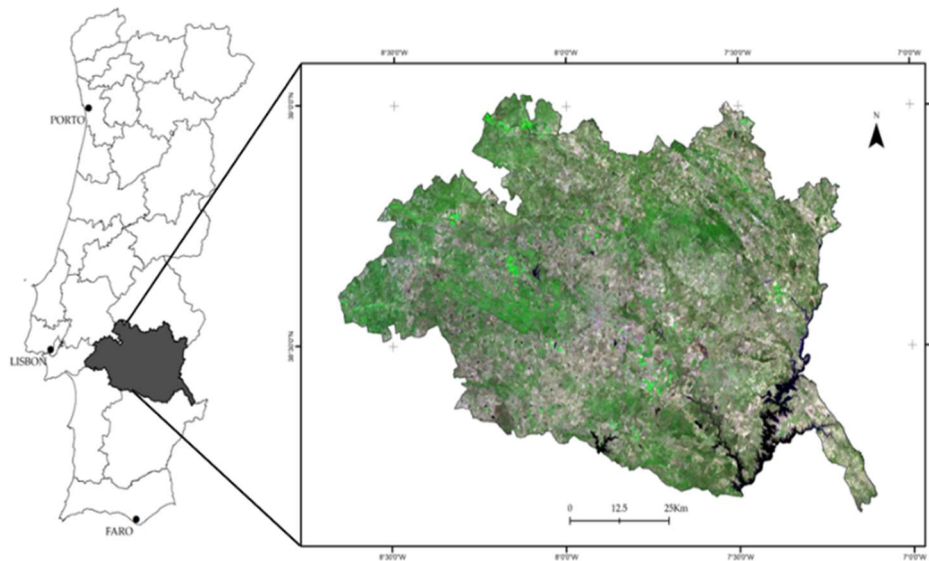


**Figure 1.** Study area in false color composite (RGB - Bands 4, 8, and 3) using Sentinel-2A image.

The landscape is dominated by agroforestry systems named “*montado*” [40]. These systems are composed by *Quercus suber* and/or *Quercus rotundifolia*, characterised by low densities and irregular spatial arrangement frequently with an understorey composed of shrubby and herbaceous species [41]. The “*montado*” is classified as a High Natural Value Agricultural System by the European Environment Agency [42] and listed in the Habitats Directive as habitats of conservation value [43]. The “*montados*” of *Quercus suber* have as their main product bark (cork) and those of *Quercus rotundifolia* fruit [44]. The species can occur in pure and mixed stands [45]. The forests of *Eucalyptus sp* and *Pinus pinea* are distributed in the area in small mosaics, occupying about 6 and 5% of the forest area, respectively [2]. The pure even aged stands of *Eucalyptus sp* are mostly intended for the production of short-fiber cellulose pulp, paper, and biomass for energy production [46]. *Pinus pinea* stands frequently pure even aged or mixed with *Quercus suber*, have as its main product edible pine nuts, which are a traditional ingredient in Mediterranean cuisine [47].

## 2.2 Data preprocessing and dataset

The S2A image processing procedures are synthetically represented in the workflow (Figure 2). Four stages were needed to generate the LULC mapping.

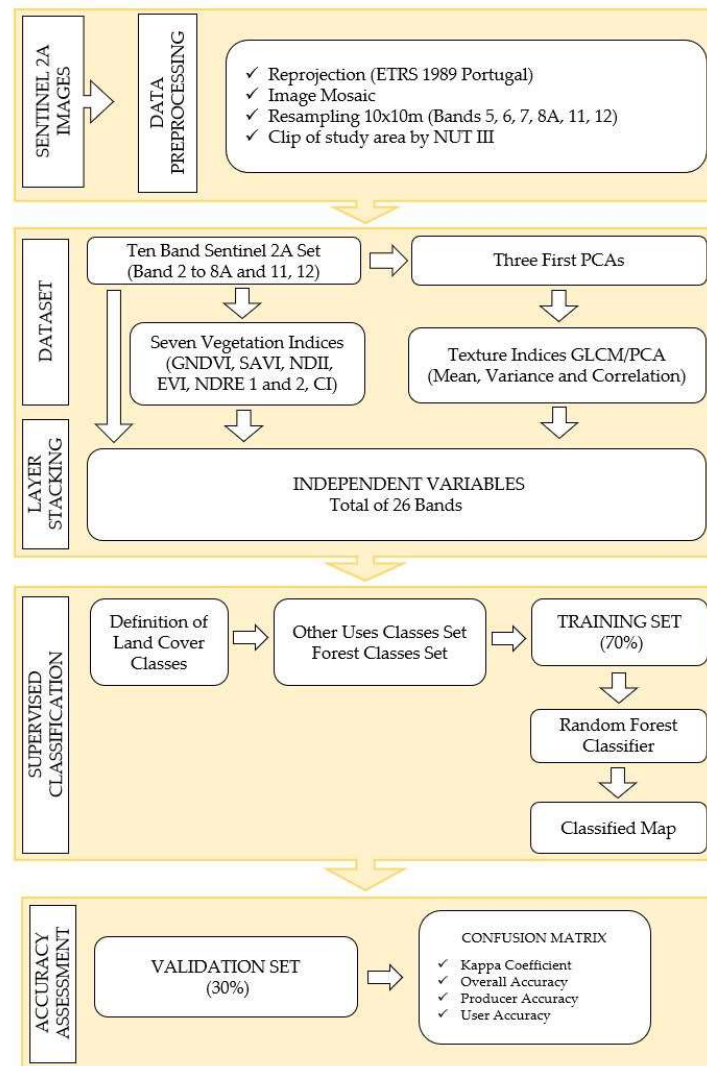


**Figure 2.** Workflow of the data processing, and validation steps implemented from Sentinel 2A images.

The acquisition of S2A products were made on the Copernicus Open Access Hub platform [48]. In total, it was necessary to use four S2A images sets to cover the entire study area. In this work, ten S2A Multispectral (MSI) band sets were used the mosaics were made per band with the ETRS 1989 - Portugal reference system. The acquisition images date was September 2, 2019, with cloud filtering of less than 10%. For forest classification studies, in the summer season, shows more probability to find images with a lower clouds covers, in addition, to increase the contrast between the spectral classes of the forest canopy cover and the layers of soil understory vegetation, which are mostly dry, in this season [13]. Thus, to have all bands with the same spatial resolution, a nearest-neighbor interpolation scaling procedure was used to reduce the 20 m bands (5, 6, 7, 8A, 11, and 12) to 10m [49].

Seven vegetation indices (VIs) were selected to extract information about the spectral vegetation behavior in relation to the ground and differentiate it from other surface targets [13,50]. The VIs used were: GNDVI, SAVI, EVI, NDII, NDRE 1 and 2, and CI (Table 1). To optimize indices texture, the Principal Component Analysis (PCA) was applied to the 10 spectral bands set of the S2A images [26,51]. PCA summarizes most of the data variation of

the ten spectral bands of S2A, compressing redundant data embedded in each spectral channel [52]. Although studies indicate that the first principal component gathers most of the information on the separability of land use classes [23,53], in this work, were used the three firsts components, they explain 99.56% of the spectral variation of the data set considered [1]. On the 3 PCA's, GLCM texture measurements (Average, Variance and Correlation), were extracted with a moving window size  $9 \times 9$ , in all directions ( $0^\circ$ ,  $45^\circ$ ,  $90^\circ$ , and  $135^\circ$ ), with quantization of 32 gray levels, based on variogram method [54,55]. In the literature, the configurations for GLCM textures and the definition of the ideal size of the moving window are still dependent on the land use characteristics and the diversity of the bands [56,57]. Thus, a window size suggested by [54] was used in this study to improve classification accuracy in heterogeneous landscapes with varying sizes of training features. Adopting a smaller window is more recommended for homogeneous terrain types and with fixed training plot sizes [58]. For these proposes was used the free software, Sentinel Application Platform (SNAP) 7.0 [59].

**Table 1.** Vegetation indices and GLCM textural measures derived from Sentinel-2A images.

Type	Description	Equation
Vegetation Indices (VIs)	GNDVI Green Normalized Difference Vegetation Index	$\frac{NIR - Green}{NIR + Green}$
	SAVI Soil Adjusted Vegetation Index	$1.5 \times \frac{NIR - Red}{8 \times (NIR + Red + 0.5)}$
	NDII Normalized Difference Infrared Index	$\frac{NIR - SWIR_1}{NIR + SWIR_1}$
	EVI Enhanced Vegetation Index	$2.5 \times \left( \frac{NIR - Red}{(NIR - 6 \times Red - (Red - 7.5 * Blue) + 1)} \right)$
	NDRE 1 Normalized Difference Red Edge Index 1	$\frac{Red\ edge\ 4 - Red\ edge\ 1}{Red\ edge\ 4 + Red\ edge\ 1}$
	NDRE 2 Normalized Difference Red Edge Index 2	$\frac{Red\ edge\ 4 - Red\ edge\ 3}{Red\ edge\ 4 + Red\ edge\ 3}$
	CI Red-edge Chlorophyll Index	$\frac{Red\ edge\ 2}{Red\ edge\ 1}$
GLCM Textural Measures	Mean Average of the grey level sum distribution of the image	$\sum_{i,j=0}^{N-1} i P_{i,j}$
	Variance Measures the dispersion (relative to the mean) of the grey level distribution	$\sum_{i,j=0}^{N-1} i P_{i,j} (i - \mu)^2$
	Correlation Measures linear greyscale dependencies in the image and describes the similarity between column or row elements in GLCM.	$\frac{\sum_{i,j=0}^{N-1} i P_{i,j} - \mu_x \mu_y}{\sigma_x \sigma_y}$

where,  $P(i,j)$  is a normalized grey-tone spatial dependence matrix such that  $\sum_{i,j=0}^{N-1} P(i,j) = 1$ ;  $i$  and  $j$  represent the rows and columns, respectively, for the measures of Mean, Variance and Correlation;  $\mu$  is the mean, for the Variance textural measure; and  $N$  is the number of distinct grey levels in the quantized image;  $\mu_x$ ,  $\mu_y$ ,  $\sigma_x$ , and  $\sigma_y$  are the means and standard deviations of  $p_x$  and  $p_y$ , respectively, for the correlation textural measure.

The software SNAP was also used to obtain the importance of each independent variable to the class separability in the classification process. To complement this information, it was computer the Jeffries–Matsushita (J–M) distance for all possible combinations of pair of classes. For this measure, with range from 0 to 2, where, the value 2 indicate the completely separability of classes, values from 1.99 to 1.5 the classes are clearly separate, between 1 and 1.5 the classes are separable with some confusion and below 1.5 the classes are not separable [11].

### 2.3 Supervised classification

#### 2.3.1 Definition of LULC classes and selection of training features

In the application of the supervised classification method, the LULC classes were defined by creating polygons (Regions of Interest – ROIs features) with uniform distribution of samples over the ground cover according to the area characteristics [30]. In the definition of training and validation samples, the prior recognition of the study area is essential for create training samples to guide the image classification process [6]. Therefore, to deliniate the ROIs features of each LULC class, auxiliary data was used to identify the classes in the reference image. Were used images from Google Sattellite integrated on the OGC Catalog Service for the Web (CSW) standard metadata catalogue service in QGIS [60] and Land Use and Occupation Map (COS) from 2018 [61]. The ROIs features were defined using the tool “Active ROI pointer” from the Semi-Automatic Classification Plugin version 7.8.34, available as open-source and free in QGIS 3.16.0 [62].

In this way, eight predominant LULC classes were defined, being four forest classes and four classes of other uses. The set of other LULC uses classes were grouped: Water surfaces: areas of soil that are covered by water; Baresoil and artificial surfaces: areas with dry vegetation cover, rock outcrops, baresoil, quarries, and urban areas, solar panel parks, greenhouse structures; Agricultural areas: irrigated crops, permanent agriculture areas (vines and olive groves); Shrub surface: correspond areas occupied mainly by shruby species spetaneous of the Mediterranean regions. Note that, in this study, we chose to include the baresoil class and urban areas in a single class (Soil and artificial surfaces). In the summer period, when there is low agriculture activity and low baresoil moisture areas, the reflectance values are higher. Thus, the low spectral separability make it dificult to separate artificial surfaces and natural surfaces without vegetation (baresoil, quarries, urban area). The forest classes set were *Eucaliptus sp.*, *Pinus pinea*, *Quercus rotundifolia*, and *Quercus suber*. Thus, ROIs features were used for the training and validation of the classification algorithm that determines discrimination rules between the different LULC classes.

#### 2.3.2 Random Forest Classification

Random Forest (RF) is a non-parametric machine learning algorithm, developed by [63], in which data set is frequently divided in two sub samples; the training and the validation. The RF builds multiple decision trees, based on random bootstrapping of training data, overcoming the overfitting generated with the Decision Trees (DT) classifier [63,64]. In the data training step, the RF operates by building several of DT, in which each division of the tree is determined using a random subset of the predictors at each node. The resulting output is predicted by the majority of unweighted “votes” for each class, averaged over all trees [32,65]. The validation data set, produces an internal and unbiased estimate of the generalization error using out-of-bag (OOB) samples [66]. One of the advantages of using RF as a classifier is the easy parameterization, the ability to manage collinear resources and high-dimensional data [67], as well as, it is robust against overfitting and outliers [68].

In this study, the free and open-source software package Orfeo ToolBox (OTB) [69], was used for the supervised classification process and for the analysis of precision statistics of the LULC mapping. OTB has a wide application of object-oriented machine learning classification algorithms, which include supervised methods such as Support Vector Machines (SVM), Artificial Neural Networks (ANN), and Random Forest (RF) [70]. Thus, the ROIs were selected by the independent stratified random selection method, where 70% were used to train the classifier, while 30% to validation, in the accuracy assessment (Table 2) [71–73]. The RF classification algorithm was applied to the 26 independent variables by the OTB 7.1.0 tool package, implemented in the QGIS 3.16.0-Hannover platform. The number of trees was 500, with a depth of 25, and the OOB error was set to 0.01 [74]. The number of trees chosen proves to be sufficient to obtain a good classification result, since higher values present similar results, have a processing time and the change of the other parameters has little influence, as they remain with an OOB error value [67,75–78].

**Table 2:** Training and validation samples for each LULC class collected as group of pixels.

Sets	LULC Classes	ROIs features Number	Pixels Number		
			70% Training	30% Validation	Total
Other Uses Classes	Water Surfaces	29	77 966	33 414	111 380
	Soil and Artificial Surfaces	29	45 829	19 641	65 470
	Agricultural surfaces	231	142 326	60 997	203 323
	Shrub Surface	192	30 867	13 229	44 096
Forest Classes	<i>Eucalyptus sp.</i>	227	119 346	51 149	170 495
	<i>Pinus pinea</i>	334	103 311	44 276	147 587
	<i>Quercus rotundifolia</i>	1 111	155 681	66 720	222 401
	<i>Quercus suber</i>	685	160 406	68 745	229 151

### 2.3.3 Accuracy Assessment

After the supervised classification step, statistics methods play an important role in assessing the accuracy of classification mapping [79]. By comparing the classified map with the reference image, using the information from the validation samples, accuracy statistics can be derived by the confusion matrix. Thus, in this study, the LULC map was evaluated by the most popular metrics (overall (OA) producer's (PA) and user's (UA) accuracies and Kappa statistics) using 30% of the samples set for validation of the reference data [80,81]. The AO, PA, and UA can be categorized as follows: very high accuracy (over 90%), high accuracy (80-89%), acceptable accuracy (70-79%), low accuracy (less than 69%) [35]. The Kappa Coefficient (k) is a measure of map accuracy most used in remote sensing, proposed by [82]. The Kappa coefficient [35,83], considers that values above 0.8 present thematic maps with a high level of agreement between the resulted map and the ground truth [82].

## 3. Results

The analysis of the spectral separability of the J-M measure revealed that when comparing the pairs of classes from the set of other uses with the forest classes, the values of J-M were 2.0, being completely separable. On the

other hand, in the comparison made between pairs of forest classes, the J-M measure presented a value of 1.9, being clearly separable.

The results for the accuracy statistics derived from the RF classifier approaches are shown in Table 3. Specifically, the OA, PA, UA and Kappa coefficient were obtained of the confusion matrix. The overall accuracy in the case of the single model was 92.16%, while the Kappa coefficient of 91.04%. The set of classes with other uses, obtained UA (commission errors) values that ranged between 93.45% and 99.92%, and PA (omission errors) value ranged between 93.78% and 99.70%. However, as the objective of this study was to show the performance of the RF algorithm for the forest classes set, the classified map is shown in Figure 2. For these classes, the UA values ranged between 80.93% and 90.00% and PA ranged between 85.79% and 89.06%.

**Table 3:** Accuracy assessment for the forest classes set obtained by RF classification.

Sets	LULC Classes	User Accuracy (UA)	Producer Accuracy (PA)
Forest Classes	<i>Eucalyptus sp.</i>	88.17	87.85
	<i>Pinus pinea</i>	89.75	89.06
	<i>Quercus rotundifolia</i>	80.93	85.79
	<i>Quercus suber</i>	90.00	86.77
Overall Accuracy (OA)	92.16		
Kappa Coefficient	91.04		

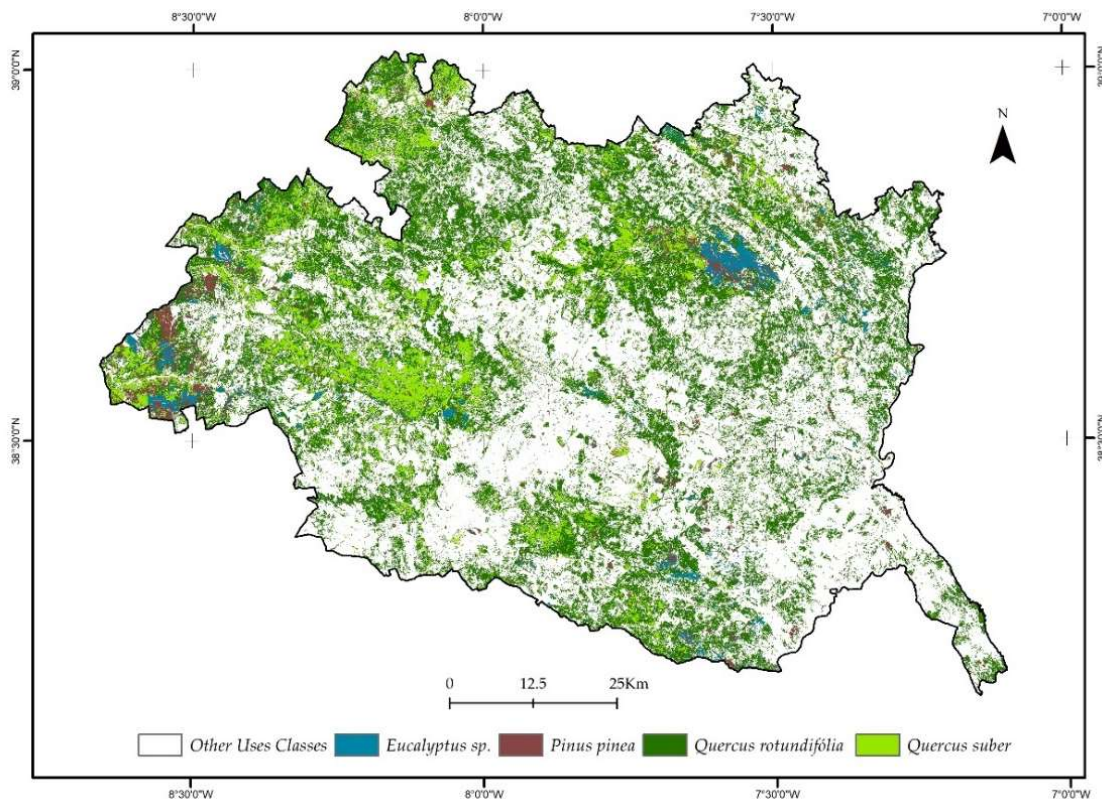


**Figure 2.** Land use mapping with forest and other uses classes from Random Forest classifier.

#### 4. Discussion

In this study, it was identified that the most important Sentinel 2 spectral bands in the classification process were the red-edges and NIR (B8) and SWIR1(B11) bands. The red-edge bands were sensitive to chlorophyll levels a and b and their variations [84–86], while NIR is a wavelength that expresses the scattering canopy radiation [85], and the SWIR detects water content variations between different forest species [87,88]. Other LULC studies have also identified the same spectral bands as important variables for the LULC classification, especially for forest classes. Studies using single-date Sentinel 2 images to classify forest species in Germany, identified that the most important bands were red-edge 1 (B5), SWIR 1 (B11), and the blue band (B2) [76]. The same way, [72] used Sentinel 2 single-date images for mapping LULC in the Roorkee region - India, identified that the NIR band (B8) had greater participation in spectral separability in forest classes with higher and lower density (N/ha). Also, [89] using Sentinel 2 images to map *Eucalyptus sp.* species, identified that the most important spectra in distinguishing the class were the green (B3), red-edge 3 (B7) red-edge 4 bands, or narrow NIR (B8A).

Among the studied vegetation indices, few indices influenced the gain in classification accuracy. The SAVI index contributed to the soil adjustment constant in the background of the vegetation signal, an important factor when it comes to studies in the dry season and in semi-arid regions [17]. In addition, EVI had a greater relationship with sensitivity to biophysical changes in the forest canopy, such as leaf pigments, such as chlorophyll and leaf nitrogen, and regions of high biomass [90]. Works similar to ours also report the low impact of vegetation indices on the accuracy of LULC studies [55,91,92]. In the Mediterranean ecosystem, [92] when analyzing the importance of including eight vegetation indices of Sentinel 2 (GNDVI Green Normalized Difference Vegetation Index; NDVI Normalized Difference Vegetation Index; NDI45 Normalized Difference Index; S2REP Sentinel-2 Red-Edge Position Index; SAVI Soil-Adjusted Vegetation Index; MSAVI2 Second Modified Soil-Adjusted Vegetation Index; BI Brightness Index and CI Color Index), in the classification of four forest classes - holm oaks (*Quercus ilex*), cork oaks (*Quercus suber*), and Eucalyptus (*E. globulus* and *E. camaldulensis*) - and four of other uses, in Badajoz province (Spain), verified that only MSAVI 2 had a participation in the accuracy gains. In the Extremadura region in Spain, [55] verified that among the eight vegetation indices (BI Brightness Index, CI Color Index, GNDVI Green Normalized Difference Vegetation Index, MSAVI2 Second Modified Soil-Adjusted Vegetation Index, NDI45 Normalized Difference Index, NDVI Normalized Difference Vegetation Index, NDWI Normalized Difference Water Index, SAVI Soil Adjusted Vegetation Index) derived from Sentinel 2 data, only CI was important in the classification process of four forest classes – ENF: Evergreen needle leaf forest (*Pinus pinaster*, *Pinus pinea*); EBF: Evergreen broadleaf forest (*Quercus rotundifolia*, *Quercus suber*) TCC: Tree Canopy Cover>60%; DHS: Evergreen broadleaf forest (*Quercus rotundifolia*, *Quercus suber*) 20<TCC>60%, and DBF: Deciduous broadleaf forest (*Quercus pyrenaica*, *Castanea sativa*) - and nine other uses, using the RF classifier. Thus, we observed that, by including only vegetation indices in LULC studies, they may not produce good accuracy results. Trong et al [91], had lower accuracy results than our study, but they showed the importance of including textures indices to improve the accuracy in the LULC classification.

In this study, the measures of variance and correlation of the GLCM textures, derived from principal components 2 and 3, were the bands of the greatest importance for the forest species classification. The GLCM metrics were more sensitive to canopy cover variation and abrupt changes in digital numbers between neighboring image pixels, which are more prominent in the dry season [93]. Furthermore, when studying forest

classes with heterogeneous and complex spatial distribution, these bands highlight the contrast in the boundaries of the stand [94]. Thus, the measure of GLCM variance had greater sensitivity in the intraclass visual borders, as it increases when it obtain higher or lower values when there is a large disparity in the gray level between pixels. On the other hand, the GLCM correlation measures are associated with the linear dependence between two neighboring pixels, and similar gray levels with higher values in areas far from edges tend to cluster [20]. Several LULC studies report that the inclusion of texture features can improve classification accuracy, as obtained in our study [3,75,76,95].

Thus, the high accuracy value and kappa coefficient shown in table 2 was achieved by the synergistic use between texture indices and spectral bands. In the individual assessment of the accuracy of each forest class, it was observed that there were some pixels that were incorrectly classified. However, a visual inspection was necessary to verify the spectral confusion points between the classified image and the reference image. Thus, when analyzing the J-M measure, was verified that all pairs of forest classes were clearly separable, with a value of 1.9. This separability was achieved by using the "Active ROI pointer" tool, which optimizes the process of marking ROIs features, which uses an algorithm that segments the image around a pixel seed, which includes spectrally homogeneous pixels in a feature [62]. The predicted regions that were incorrectly classified are located in mixed stands or with low spatial distribution, and also in transition zones between stands. In Mediterranean ecosystems, the classifier may have difficulty identifying the spatial arrangements of species specially in the montado systems, as species have high variability in their distribution pattern [13,96,97]. On the other hand, it can be noted that the class of *Q. rotundifolia* presented a lower user and producer accuracy than *Q. suber*. This reduction in individual accuracies is due to the spectral similarity between the Agricultural surfaces and Shrub Surface classes. Some *Q. rotundifolia* pixels were incorrectly classified in boundaries of areas of vineyards and olive groves which have very similar spectral ranges. Regarding Shrub Surface classes, spectral confusion occurred mainly in regions where the shrub signal was dominant in the reflectance of young *Q. rotundifolia*. The dominance of reflectance of understory vegetation or soils was also observed in growing forest stands, due to gaps between a sparse canopy structure [98,99]. Among the pairs of classes of *Eucalyptus sp.* and *P. pinea*, misclassifications were more frequent in riparian forests and orchards with spectrally similar signs. In addition, small fragments from the second rotation of *Eucalyptus sp.* and young *P. pinea* plantations influenced the signal change due to spatially open canopies.

In general, in our study the RF classifier had good performance in overall accuracy and kappa statistics, reaching values similar or higher to the studies of [72,76,100]. Immitzer et al. [76] obtained an overall accuracy of 66% and a kappa coefficient of 58% when classifying the species of *P. abies*, *P. silvestris*, *Larix decidua*, *Abies alba*, *Fagus sylvatica*, and *Quercus sp.*, using RF classifier. LULC studies in the Mediterraneo ecosystem, [72] and [100], also reported an overall accuracy of 84% and 93% with a kappa coefficient of 83% and 73%, respectively. Other LULC studies using Sentinel 2 images can be found in [101]. One of the alternatives to improve the classification results of our work would be to include Sentinel-2 multitemporal images and use the synergy between Sentinel 1 data, as shown in the studies [1,3,102–104]. Although the different window sizes test was not one of the objectives of this study, the mapping of forest classes in different window sizes can be an alternative to classification accuracy assessment.

## 5. Conclusion

In this study, the RF algorithm produced a good accuracy for LULC classes for Central Alentejo, reaching an overall accuracy of 92.16% and a Kappa coefficient of 91.04%. In addition, images acquired in the summer contributed to a good classification due to the lower occurrence of clouds and the distinctive spectral behaviour of the understory as well as between forest and other uses.

For the forest classes set, the RF model performed well, despite the complexity of forest occupation in Central Alentejo, with high intraclass variability.

The results confirm the potential of Sentinel 2A data in LULC mapping. The Sentinel-2 spectral bands and texture indices had the greatest contribution to the classification results. The images were useful in developing spatial estimates of forest cover and species distribution in complex and heterogeneous landscapes.

**Funding:** This work is funded by Programa Operativo de Cooperação Transfronteiriça Espanha-Portugal (POCTEP); project CILIFO – Centro Ibérico para la Investigación y Lucha contra Incendios Forestales (0753\_CILIFO\_5\_E) and by FCT- Foundation for Science and Technology under the Project UIDB/05183/2020.

## 6 Reference

1. Chatziantoniou A.; Petropoulos G.P.; Psomiadis E. Co-Orbital Sentinel 1 and 2 for LULC mapping with emphasis on wetlands in a mediterranean setting based on machine learning. *Remote Sens.* **2017**; 9 (12):1–19. DOI:10.3390/rs9121259
2. ICNF. 6.º Inventário Florestal Nacional (IFN6). Relatório Final; ICNF–Instituto da Conservação da Natureza e das Florestas: Lisboa, Portugal, **2019**.
3. Vasilakos C.; Kavrouidakis D.; Georganta A. Machine learning classification ensemble of multitemporal Sentinel-2 images: The case of a mixed mediterranean ecosystem. *Remote Sens.* **2020**; 12 (12): 1–25. DOI:10.3390/rs12122005
4. Peñuelas, J.; Gracia, C.; Alistair Jump, I.F.; Carnicer, J.; Coll, M.; Lloret, F.; Yuste, J.C.; Estiarte, M.; Rutishauser, T.; Ogaya, R. Introducing the climate change effects on Mediterranean forest ecosystems: Observation, experimentation, simulation, and management. *Forêt Médit.* **2010**, 31: 357–362.
5. Friedl, M.A.; McIver, D.K.; Hodges, J.C.F.; Zhang, X.Y.; Muchoney, D.; Strahler, A.H.; et al. Global land cover mapping from MODIS: Algorithms and early results. *Remote Sens Environ.* **2002**; 83 (1–2); 287–302. DOI:10.1016/S0034-4257(02)00078-0
6. De Luca, G.; Silva, J.M.N.; Cerasoli, S.; Araújo, J.; Campos, J.; Di Fazio, S.; et al. Object-based land cover classification of cork oak woodlands using UAV imagery and Orfeo Toolbox. *Remote Sens.* **2019**;11(10): 1–22. DOI:10.3390/rs11101238
7. Chen, Y.; Guerschman, J.P.; Cheng, Z.; Guo L. Remote sensing for vegetation monitoring in carbon capture storage regions: A review. *Appl Energy.* **2019**; 240: 312–26. DOI:10.1016/j.apenergy.2019.02.027
8. Isbaex, C.; Coelho, A.M. The potential of Sentinel-2 satellite images for land-cover/land-use and forest biomass estimation: A review. In: Gonçalves, A.C.; Sousa, A.M.O. *Forest Biomass – From Trees to Energy*. IntechOpen. **2020**. pp1-25. DOI:10.5772/intechopen.93363
9. ESA. Sentinel-2 User Handbook. Vol. 2. European Space Agency ESA Standard Document. Paris, France; 2015. p. 64. DOI: 10.1021/ie51400a018
10. Hawryło, P.; Bednarz, B.; Wężyk, P.; Szostak M. Estimating defoliation of Scots pine stands using machine learning methods and vegetation indices of Sentinel-2. *Eur J Remote Sens.* **2018**; 51 (1): 194–204. DOI:10.1080/22797254.2017.1417745
11. Mananze, S.; Pôças, I.; Cunha, M. Mapping and assessing the dynamics of shifting agricultural landscapes using google earth engine cloud computing, a case study in Mozambique. *Remote Sens.* **2020** ;12 (8): 1–23. DOI:10.3390/RS12081279
12. Tassi, A.; Vizzari, M. Object-Oriented LULC Classification in Google Earth Learning Algorithms. *Remote Sens.* **2020**; 12: 1–17. DOI:10.3390/rs12223776

13. Godinho, S.; Guiomar, N.; Gil A. Estimating tree canopy cover percentage in a mediterranean silvopastoral systems using Sentinel-2A imagery and the stochastic gradient boosting algorithm. *Int J Remote Sens.* **2018**; 39 (14): 46: 40–62. DOI:10.1080/01431161.2017.1399480
14. Gitelson, A.A.; Kaufman, Y.J.; Merzlyak, M.N. Use of a green channel in remote sensing of global vegetation from EOS- MODIS. *Remote Sens Environ.* **1996**; 58 (3): 289–98. DOI:10.1016/S0034-4257(96)00072-7
15. Liu, H.Q.; Huete, A. Feedback based modification of the NDVI to minimize canopy background and atmospheric noise. *IEEE Trans Geosci Remote Sens.* **1995**; 33 (2): 457–65. DOI:10.1109/36.377946
16. Hunt, E.R.; Rock, B.N. Detection of changes in leaf water content using Near- and Middle-Infrared reflectances. *Remote Sens Environ.* **1989**; 30 (1): 43–54. DOI:10.1016/0034-4257(89)90046-1
17. Huete, A.R. A Soil-Adjusted Vegetation Index (SAVI). *Remote Sens Environ.* **1988**; 25 (1): 295–309. DOI:10.1016/0034-4257(88)90106-X
18. Navarro, G.; Caballero, I.; Silva, G.; Parra, P.C.; Vázquez, Á.; Caldeira, R. Evaluation of forest fire on Madeira Island using Sentinel-2A MSI imagery. *Int J Appl Earth Obs Geoinf.* **2017**; 58: 97–106. DOI:10.1016/j.jag.2017.02.003
19. Zarco-Tejada, P.J.; Miller, J.R.; Noland, T.L.; Mohammed, G.H.; Sampson, P.H. Scaling-up and model inversion methods with narrowband optical indices for chlorophyll content estimation in closed forest canopies with hyperspectral data. *IEEE Trans Geosci Remote Sens.* **2001**; 39 (7): 1491–507. DOI:10.1109/36.934080
20. Hall-Beyer, M. Practical guidelines for choosing GLCM textures to use in landscape classification tasks over a range of moderate spatial scales. *Int J Remote Sens.* **2017**; 38 (5): 1312–1338. DOI:10.1080/01431161.2016.1278314
21. Haralick, R.M.; Shanmugam, K.; Dinstein, I. Textural Features for Image Classification. *SEG Tech Progr Expand Abstr.* **1973**; 3: 610–621. DOI:10.1190/segam2015-5927230.1
22. Julesz, B. Experiments in the visual perception of texture. *Sci Am.* **1975**; 232 (4): 34–43. DOI:10.1038/scientificamerican0475-34
23. Kupidura, P. The comparison of different methods of texture analysis for their efficacy for land use classification in satellite imagery. *Remote Sens.* **2019**; 11:1–20. DOI:10.3390/rs11101233
24. Ferro, C.J.S.; Warner, T.A. Scale and texture in digital image classification. *Photogramm Eng Remote Sensing.* **2002**; 68 (1): 51–63. DOI:10.33915/etd.93%0A%0A
25. Colombo, R.; Bellingeri, D.; Fasolini, D.; Marino, C. M. Retrieval of leaf area index in different vegetation types using high resolution satellite data. *Remote Sens Environ.* **2003**; 86 (1): 120–31. DOI:10.1016/S0034-4257(03)00094-4
26. Jolliffe, I.T.; Cadima, J. Principal component analysis: A review and recent developments. *Philos Trans R Soc A Math Phys Eng Sci.* **2016**; 374 (2065): 1–16. DOI:10.1098/rsta.2015.0202
27. Gómez, C.; White, J.C.; Wulder, M.A. Optical remotely sensed time series data for land cover classification: A review. *ISPRS J Photogramm Remote Sens.* **2016**; 116: 55–72. DOI:10.1016/j.isprsjprs.2016.03.008
28. Rodriguez-Galiano, V.F.; Ghimire, B.; Rogan, J.; Chica-Olmo, M.; Rigol-Sanchez, J.P. An assessment of the effectiveness of a random forest classifier for land-cover classification. *ISPRS J Photogramm Remote Sens.* **2012**; 67 (1): 93–104. DOI:10.1016/j.isprsjprs.2011.11.002
29. Hernandez, I.; Benevides, P.; Costa, H.; Caetano, M. Exploring sentinel-2 for land cover and crop mapping in portugal. *Int Arch Photogramm Remote Sens Spat Inf Sci - ISPRS Arch.* **2020**; 43 (B3): 83–89. DOI:10.5194/isprs-archives-XLIII-B3-2020-83-2020
30. Ma, Ma L, Li M, Ma X, Cheng L, Du P, Liu Y. A review of supervised objectbased land-cover image classification. *ISPRS J Photogramm Remote Sens.* **2017**; 130: 277-293. DOI:10.1016/j.isprsjprs.2017.06.001
31. Lu, D.; Weng, Q. A survey of image classification methods and techniques for improving classification performance. *Int J Remote Sens.* **2007**; 28 (5): 823–870. DOI:10.1080/01431160600746456

32. Gislason, P.O.; Benediktsson, J.A.; Sveinsson, J. R. Random forests for land cover classification. *Pattern Recognit Lett.* **2006**; *27* (4): 294–300. DOI:10.1016/j.patrec.2005.08.011
33. Jin, Y.; Liu, X.; Chen, Y.; Liang, X. Land-cover mapping using Random Forest classification and incorporating NDVI time-series and texture: a case study of central Shandong. *Int J Remote Sens.* **2018**; *39* (23): 8703–8723. DOI:10.1080/01431161.2018.1490976
34. Praticò, S.; Solano, F.; Di Fazio, S.; Modica, G. Machine learning classification of mediterranean forest habitats in google earth engine based on seasonal sentinel-2 time-series and input image composition optimisation. *Remote Sens.* **2021**; *13* (4): 1–28. DOI:10.3390/rs13040586
35. Story, M.; Congalton, R.G. Remote sensing brief accuracy assessment: A user's perspective. *Photogrammetric Engineering and Remote Sensing.* **1986**; *52* (3): 397-399
36. Smits, P.C.; Dellepiane, S.G.; Schowengerdt, R.A. Quality assessment of image classification algorithms for land-cover mapping: A review and a proposal for a cost-based approach. *Int J Remote Sens.* **1999**; *20* (8): 1461–1486. DOI:10.1080/014311699212560
37. Foody, G.M. Status of land cover classification accuracy assessment. *Remote Sens Environ.* **2002**; *80* (1): 185-201. DOI: 10.1016/S0034-4257(01)00295-4
38. Liu, C.; Frazier, P.; Kumar, L. Comparative assessment of the measures of thematic classification accuracy. *Remote Sens Environ.* **2007**; *107* (4): 606-616. DOI: 10.1016/j.rse.2006.10.010
39. Divisão Geral do Território – DGT. 2020. Carta Administrativa Oficial de Portugal. Available from: <https://www.dgterritorio.gov.pt/cartografia/cartografia-tematica/caop>
40. Sousa, A.M.O.; Gonçalves, A.C.; da Silva, J. R. M. Above-Ground Biomass Estimation with High Spatial Resolution Satellite Images. In *Biomass Volume Estimation and Valorization for Energy*; IntechOpen: London, UK, **2017**. DOI:10.5772/65665
41. Pinto-Correia, T.; Ribeiro, N.; Sá-Sousa, P. Introducing the montado, the cork and holm oak agroforestry system of Southern Portugal. *Agrofor Syst.* **2011**; *82* (2): 99–104. DOI:10.1007/s10457-011-9388-1
42. Paracchini, M.L.; Petersen, J-E.; Hoogeveen, Y.; Bamps, C.; Burfield, I.; Swaay, C. V. High Nature Value Farmland in Europe - An Estimate of the Distribution Patterns on the Basis of Land Cover and Biodiversity Data. Institute for Environment and Sustainability Office for Official Publications of the European Communities Luxembourg. 2008: 1–102. DOI:10.2788/8891
43. Catry, F.X.; Moreira, F.; Pausas, J.G.; Fernandes, P.M.; Rego, F.; Cardillo, E.; et al. Cork oak vulnerability to fire: The role of bark harvesting, tree characteristics and abiotic factors. *PLoS One.* **2012**; *7*(6): 1–9. DOI:10.1371/journal.pone.0039810
44. Barrico, L.; Rodríguez-Echeverría, S.; Freitas, H. Diversity of soil basidiomycete communities associated with *Quercus suber* L. in Portuguese montados. *Eur J Soil Biol.* **2010**; *46* (5): 280–287. DOI:10.1016/j.ejsobi.2010.05.001
45. Gonçalves, A.C.; Sousa, A.M.O.; Mesquita, P.G. Estimation and dynamics of above ground biomass with very high resolution satellite images in *Pinus pinaster* stands. *Biomass and Bioenergy.* **2017**; *106*: 146–154. DOI:10.1016/j.biombioe.2017.08.026
46. The Navigator Company. The Newsletter: Conhecer o Eucalipto. 2020. Available from: [http://www.thenavigatorcompany.com/var/ezdemo\\_site/storage/original/application/a5eb5d7c3491f0ef009d7bcde3c80958.pdf](http://www.thenavigatorcompany.com/var/ezdemo_site/storage/original/application/a5eb5d7c3491f0ef009d7bcde3c80958.pdf)
47. Sousa, J.L.C.; Ramos, P.A.B.; Freire, C.S.R.; Silva, A.M.S.; Silvestre, A.J.D. Chemical composition of lipophilic bark extracts from *pinus pinaster* and *pinus pinea* cultivated in Portugal. *Appl Sci.* **2018**; *8* (12): 1-11. DOI:10.3390/app8122575
48. European Space Agency (ESA). Copernicus Open Access Hub. 2020. Available from: <https://scihub.copernicus.eu/>
49. Zheng, H.; Du, P.; Chen, J.; Xia, J.; Li, E.; Xu, Z; et al. Performance evaluation of downscaling sentinel-2 imagery for Land Use and Land Cover classification by spectral-spatial features. *Remote Sens.* **2017**; *9* (12): 1-17. DOI:10.3390/rs9121274
50. Wiesmair, M.; Feilhauer, H.; Magiera, A.; Otte, A.; Waldhardt, R. Estimating vegetation cover from high-resolution satellite data to assess grassland degradation in the Georgian Caucasus. *Mt Res Dev.* **2016**; *36* (1): 56–65. DOI:10.1659/MRD-JOURNAL-D-15-00064.1

51. Jensen, J.R. *Remote Sensing of the Environment: An Earth Resource Perspective 2/e*; Pearson Education: Delhi, India, 2009.
52. Eklundh, L.; Singh, A. A comparative analysis of standardised and unstandardised principal components analysis in remote sensing. *Int J Remote Sens.* **1993**; 14 (7): 1359–1370. DOI:10.1080/01431169308953962
53. Waser, L.T.; Küchle, r M.; Jütte, K.; Stampfer, T. Evaluating the potential of worldview-2 data to classify tree species and different levels of ash mortality. *Remote Sens.* **2014**; 6: 4515–4545. DOI: <https://www.mdpi.com/2072-4292/6/5/4515>
54. Szantoi, Z.; Escobedo, F.; Abd-Elrahman, A.; Smith, S.; Pearlstine, L. Analyzing fine-scale wetland composition using high resolution imagery and texture features. *Int J Appl Earth Obs Geoinf.* **2013**; 23 (1): 204–212. DOI:10.1016/j.jag.2013.01.003
55. Fragoso-Campón, L.; Quirós, E.; Gallego, J. A.G. Optimization of land cover mapping through improvements in Sentinel-1 and Sentinel-2 image dimensionality and data mining feature selection for hydrological modeling. *Stoch Environ Res Risk Assess.* **2021**: 1–27. DOI:10.1007/s00477-021-02014-z
56. Franklin, S.E.; Hall, R.J.; Moskal, L.M.; Maudie, A.J.; Lavigne, M.B. Incorporating texture into classification of forest species composition from airborne multispectral images. *Int J Remote Sens.* **2000**; 21 (1): 61–79. DOI:10.1080/014311600210993
57. Dorigo, W.; Lucieer, A.; Podobnikar, T; Carni, A. Mapping invasive Fallopia japonica by combined spectral, spatial, and temporal analysis of digital orthophotos. *Int J Appl Earth Obs Geoinf.* **2012**; 19 (1): 185–195. DOI:10.1016/j.jag.2012.05.004
58. Hu, Y.; Xu, X.; Wu, F.; Sun, Z.; Xia, H.; Meng Q.; et al. Estimating Forest Stock Volume in Hunan Province, China, by Integrating In Situ Plot ,Data, Sentinel-2 Images, and Linear and Machine Learning Regression Models. *Remote Sens.* **2020**; 12 (1): 1–23. DOI:10.3390/rs12010186
59. European Space Agency (ESA). Sentinel Application Platform- SNAP. 2021. Available from:<https://step.esa.int/main/download/snap-download/>.
60. Documentation for Qgis. MetaSearch Catalog Plugin. 2021. Available from:[https://docs.qgis.org/2.8/en/docs/user\\_manual/plug](https://docs.qgis.org/2.8/en/docs/user_manual/plug).
61. Divisão Geral do Território – DGT. Carta de Uso e Ocupação do Solo - COS 2018. 2020. Available from:<https://www.dgterritorio.gov.pt/Carta-de-Uso-e-Ocu>.
62. Congedo, L. Semi-Automatic Classification Plugin Documentation Release 6.0.1.1. 2018: 1-203. DOI:10.13140/RG.2.2.29474.02242/1automaticclassificationmanual-v4.pdf
63. Breiman, L. Random forests. *Mach. Learn.* **2001**, 45, 5–32. DOI:10.1201/9780429469275-8
64. Silveira, E.M.O; Silva, S.H.G.; Acerbi-Junior, F.W.; Carvalho, M.C.; Carvalho, L.M.T.; Scolforo, J.R.S.; et al. Object-based random forest modelling of aboveground forest biomass outperforms a pixel-based approach in a heterogeneous and mountain tropical environment. *Int J Appl Earth Obs Geoinf.* **2019**; 78: 175–188. DOI:10.1016/j.jag.2019.02.004
65. Pal, M. Random forest classifier for remote sensing classification. *Int J Remote Sens.* **2005**; 26 (1): 217–222. DOI: 10.1080/01431160412331269698
66. Shaik, A.B.; Srinivasan, S. A brief survey on random forest ensembles in classification model. Vol. 56, Lecture Notes in Networks and Systems. *Springer Singapore.* **2019**: 253–260. DOI: 10.1007/978-981-13-2354-6\_27
67. Pelletier, C.; Valero, S.; Inglada, J.; Champion, N.; Dedieu, G. Assessing the robustness of Random Forests to map land cover with high resolution satellite image time series over large areas. *Remote Sens Environ.* **2016**; 187: 156–68. DOI:10.1016/j.rse.2016.10.010
68. Liaw, A.; Wiener, M. Classification and regression by random forest. *R News.* **2002**, 2, 18–22.
69. Orfeo ToolBox (OTB). 2021. Available from: <https://www.orfeo-toolbox.org/>.
70. Cresson, R.; Grizonnet, M.; Michel, J. Orfeo ToolBox Applications. *QGIS Generic Tools.* **2018**; 1: 151–242. DOI:10.1002/9781119457091.ch5
71. Adam, E.; Mutanga, O.; Odindi, J., Abdel-Rahman E.M. Land-use/cover classification in a heterogeneous coastal landscape

- using RapidEye imagery: evaluating the performance of random forest and support vector machines classifiers. *Int J Remote Sens.* **2014**;35(10): 3440–3458. DOI:10.1080/01431161.2014.903435
72. Saini, R.; Ghosh, S.K. Crop Classification on Single Date Sentinel-2 Imagery Using Random Forest and Support Vector Machine. *ISPRS - Int Arch Photogramm Remote Sens Spat Inf Sci.* **2018**; 5: 683–688. DOI:10.5194/isprs-archives-xlii-5-683-2018
73. Lim J.; Kim K.M.; Jin R. Tree species classification using hyperion and sentinel-2 data with machine learning in South Korea and China. *ISPRS Int J Geo-Information.* **2019**; 8 (150): 1–23. DOI:10.3390/ijgi8030150
74. Tian, F.; Yang, L.; Lv, F.; Zhou, P. Predicting liquid chromatographic retention times of peptides from the *Drosophila melanogaster* proteome by machine learning approaches. *Anal Chim Acta.* **2009**; 644: 10–16. DOI:10.1016/j.aca.2009.04.010
75. Thanh Noi, P.; Kappas, M. Comparison of Random Forest, k-Nearest Neighbor, and Support Vector Machine Classifiers for Land Cover Classification Using Sentinel-2 Imagery. *Sensors (Basel).* **2017**; 18 (1): 1–20. DOI:10.3390/rs9121259
76. Immitzer, M.; Vuolo, F.; Atzberger, C. First experience with Sentinel-2 data for crop and tree species classifications in central Europe. *Remote Sens.* **2016**; 8 (3): 1–27. DOI:10.3390/rs8030166
77. Maxwell, A.E.; Warner, T.A.; Fang F. Implementation of machine-learning classification in remote sensing: An applied review. *Int J Remote Sens.* **2018**; 39 (9): 2784–817. DOI:10.1080/01431161.2018.1433343
78. Hunt, M.L.; Blackburn, G.A.; Carrasco, L.; Redhead, J.W.; Rowland, C.S. High resolution wheat yield mapping using Sentinel-2. *Remote Sens Environ.* **2019**; 233: 1–15. DOI:10.1016/j.rse.2019.111410
79. Thyagarajan, K.K.; Vignesh, T. Soft Computing Techniques for Land Use and Land Cover Monitoring with Multispectral Remote Sensing Images: A Review. *Arch Comput Methods Eng.* **2019**; 26 (2): 275–301. DOI:10.1007/s11831-017-9239-y
80. FAO. Map accuracy assessment and area estimation: A practical guide. In: National Forest Monitoring Assessment Working Paper No. 46/E. Rome, Italy: Food and Agriculture Organization of the United Nations; 2016. p. 69. Available from: <http://www.fao.org/3/ai5601e.pdf>
81. Xiong, J.; Thenkabail, P.S.; Tilton, J. C.; Gumma, M.K.; Teluguntla, P.; Oliphant, A.; et al. Nominal 30-m cropland extent map of continental Africa by integrating pixel-based and object-based algorithms using Sentinel-2 and Landsat-8 data on google earth engine. *Remote Sens.* **2017**; 9 (10): 1–27. DOI:10.3390/rs9101065
82. Landis, J.R.; Koch, G.G. The Measurement of Observer Agreement for Categorical Data. *Biometrics.* 1977; 33 (1): 159–174. DOI:10.2307/2529310
83. Foody, G.M.; Mathur A. Toward intelligent training of supervised image classifications: Directing training data acquisition for SVM classification. *Remote Sens Environ.* **2004**; 93 (1–2):107–117. DOI:10.1016/j.rse.2004.06.017
84. Zarco-Tejada, P.J.; Hornero, A.; Beck, .P.S.A.; Kattenborn, T.; Kempeneers, P.; Hernández-Clemente, R. Chlorophyll content estimation in an open-canopy conifer forest with Sentinel-2A and hyperspectral imagery in the context of forest decline. *Remote Sens Environ.* **2019**; 223: 320–335. DOI:10.1016/j.rse.2019.01.031
85. Clevers, J.G.P.W.; Gitelson, A.A. Remote estimation of crop and grass chlorophyll and nitrogen content using red-edge bands on sentinel-2 and -3. *Int J Appl Earth Obs Geoinf.* **2013**; 23(1): 344–351. DOI:10.1016/j.jag.2012.10.008
86. Adamczyk, J.; Osberger, A. Red-edge vegetation indices for detecting and assessing disturbances in Norway spruce dominated mountain forests. *Int J Appl Earth Obs Geoinf.* **2015**; 37: 90–99. DOI:10.1016/j.jag.2014.10.013
87. Bolyn, C.; Michez, A.; Gaucher, P.; Lejeune, P.; Bonnet, S. Forest mapping and species composition using supervised per pixel classification of sentinel-2 imagery. *Biotechnol Agron Soc Environ.* **2018**; 22(3): 172–187.
88. Rautiainen, M.; Lukeš, P.; Homolová, L.; Hovi, A.; Pisek, J.; Mõttus, M. Spectral properties of coniferous forests: A review of in situ and laboratory measurements. *Remote Sens.* **2018**; 10 (2):1–28. DOI:10.3390/rs10020207
89. Sibanda, M.; Mutanga, O.; Rouget, M. Examining the potential of Sentinel-2 MSI spectral resolution in quantifying above ground

- biomass across different fertilizer treatments. *ISPRS J Photogramm Remote Sens.* 2015; 110: 55–65. DOI:10.1016/j.isprsjprs.2015.10.005
90. Solymosi, K.; Kövér, G.; Romvári, R. The Progression of Vegetation Indices: a Short Overview. *Acta Agrar Kaposváriensis.* 2019;23(1): 75–90. DOI:10.31914/aak.2264
91. Trong, H.N.; Nguyen, T.D.; Kappas, M. Land Cover and Forest Type Classification by Values of Vegetation Indices and Forest Structure of Tropical Lowland Forests in Central Vietnam. *Int J For Res.* 2020; 2020: 1–18. DOI: 10.1155/2020/8896310
92. Fragoso-Campón, L.; Quirós E.; Mora, J.; Gallego, J.A.G.; Durán-Barroso, P. Overstory-understory land cover mapping at the watershed scale: accuracy enhancement by multitemporal remote sensing analysis and LiDAR. *Environ Sci Pollut Res.* 2020; 27 (1): 75–88. DOI:10.1007/s11356-019-04520-8
93. Numbisi, F.N.; Van Coillie, F.; De Wulf, R. Multi-date sentinel SAR image textures discriminate perennial agroforests in a tropical forest-savannah transition landscape. *Int Arch Photogramm Remote Sens Spat Inf Sci - ISPRS Arch.* 2018; 42 (1): 339–346. DOI:10.5194/isprs-archives-XLII-1-339-2018
94. Park, Y.; Guldmann, J.M. Measuring continuous landscape patterns with Gray-Level Co-Occurrence Matrix (GLCM) indices: An alternative to patch metrics? *Ecol Indic.* 2020; 109: 1–18. DOI:10.1016/j.ecolind.2019.105802
95. Forkuor, G.; Benewinde, Zoungrana, J.B.; Dimobe, K.; Ouattara, B.; Vadrevu, K.P.; Tondoh, J.E. Above-ground biomass mapping in West African dryland forest using Sentinel-1 and 2 datasets - A case study. *Remote Sens Environ.* 2020; 236; 111496: 1-15. DOI: 10.1016/j.rse.2019.111496
96. Sousa, A.M.O.; Gonçalves, A.C.; Mesquita, P.; Marques da Silva, J.R. Biomass estimation with high resolution satellite images: A case study of *Quercus rotundifolia*. *ISPRS J Photogramm Remote Sens.* 2015; 101: 69–79. DOI:10.1016/j.isprsjprs.2014.12.004
97. Macedo, F.L.; Sousa, A.M.O.; Gonçalves, A.C.; Marques da Silva, J.R.; Mesquita P.A.; Rodrigues R.A.F. Above-ground biomass estimation for *Quercus rotundifolia* using vegetation indices derived from high spatial resolution satellite images. *Eur J Remote Sens.* 2018;51(1); pp 932–944. DOI: 10.1080/22797254.2018.1521250
98. Joyce, S.; Olsson, H. Monitoring forest growth using long time series of satellite data. *Int Arch Photogramm Remote Sens Spat Inf Sci - ISPRS Arch.* 2000; 33: 1081–1088.
99. Nilson, T.; Rautiainen, M.; Pisek, J.; Peterso, U. Seasonal Reflectance Courses of Forests. *New Adv Contrib to For Res.* 2012: 33–58. DOI:10.5772/34962
100. Çağlayan, S.D.; Leloglu, U.M.; Ginzler, C.; Psomas, A.; Zeydanlı, U.S.; Bilgin, C.C.; et al. Species level classification of Mediterranean sparse forests-maquis formations using Sentinel-2 imagery. *Geocarto Int.* 2020; 0 (0): 1–20. DOI:10.1080/10106049.2020.1783581
101. Phiri, D.; Simwanda, M.; Salekin, S.; Ryirenda, V.R.; Murayama, Y.; Ranagalage, M.; et al. Remote sensing Sentinel-2 Data for Land Cover / Use Mapping : A Review. *Remote Sens.* 2019; 42 (3):1–35. DOI:10.3390/rs12142291
102. Nelson, M. Evaluating Multitemporal Sentinel-2 Data for Forest Mapping Using Random Forest; Stockholm University: Diva, Sweden, 2017.
103. Tavares, P.A.; Beltrão, N.E.S.; Guimarães, U.S.; Teodoro, A.C. Integration of sentinel-1 and sentinel-2 for classification and LULC mapping in the urban area of Belém, eastern Brazilian Amazon. *Sensors (Switzerland).* 2019; 19 (5): 1–20. DOI:10.3390/s19051140
104. Mngadi, M.; Odindi, J.; Peerbhay, K.; Mutanga, O. Examining the effectiveness of Sentinel-1 and 2 imagery for commercial forest species mapping. *Geocarto Int.* 2021; 36 (1): 1–12. DOI:10.1080/10106049.2019.1585483